

# Catalysis Science & Technology

Accepted Manuscript



This article can be cited before page numbers have been issued, to do this please use: M. Tinoco, S. Fernandez-Garcia, A. Villa, J. M. Gonzalez-Leal, G. Blanco, A. B. Hungria, L. Jiang, L. Prati, J. J. Calvino and X. Chen, *Catal. Sci. Technol.*, 2019, DOI: 10.1039/C9CY00273A.



This is an Accepted Manuscript, which has been through the Royal Society of Chemistry peer review process and has been accepted for publication.

Accepted Manuscripts are published online shortly after acceptance, before technical editing, formatting and proof reading. Using this free service, authors can make their results available to the community, in citable form, before we publish the edited article. We will replace this Accepted Manuscript with the edited and formatted Advance Article as soon as it is available.

You can find more information about Accepted Manuscripts in the [author guidelines](#).

Please note that technical editing may introduce minor changes to the text and/or graphics, which may alter content. The journal's standard [Terms & Conditions](#) and the ethical guidelines, outlined in our [author and reviewer resource centre](#), still apply. In no event shall the Royal Society of Chemistry be held responsible for any errors or omissions in this Accepted Manuscript or any consequences arising from the use of any information it contains.

## Selective oxidation of glycerol on morphology controlled ceria nanomaterials

Miguel Tinoco,<sup>a</sup> Susana Fernandez-Garcia,<sup>a</sup> Alberto Villa,<sup>b</sup> Juan M. Gonzalez,<sup>c</sup> Ginesa Blanco,<sup>a</sup> Ana B. Hungria,<sup>a</sup> Lei Jiang,<sup>d</sup> Laura Prati,<sup>b</sup> Jose J. Calvino,<sup>a</sup> Xiaowei Chen<sup>a,\*</sup>

Received 00th January 20xx,  
Accepted 00th January 20xx

DOI: 10.1039/x0xx00000x

www.rsc.org/

**Ceria** has attracted great interest in heterogeneous catalysis due to its facile exchange between Ce<sup>3+</sup> and Ce<sup>4+</sup>. In particular, in this work it is reported, for the first time, that morphology controlled ceria without any addition of other metal exhibits catalytic activity for the selective oxidation of glycerol. Singularly, ceria nanorods present the highest catalytic activity among all tested materials, which can be attributed to their highest surface area. Nevertheless, surface crystallography plays a key role in determining the catalytic activity and selectivity of these nanocatalysts, as proven by TEM, Raman and XPS analyses. In particular, the development of {111} ceria nanofacets on ceria nanocubes strongly affects both activity and selectivity in the selective oxidation of glycerol. On the other hand, Ce<sup>3+</sup> surface content cannot be discarded as an important factor in the catalytic activity of ceria nanoparticles for this specific redox reaction.

### 1. Introduction

Since the beginning of this century, the selective oxidation of glycerol to high-value chemicals with molecular oxygen has been extensively studied. Glycerol is the main by-product from the production of biodiesel,<sup>1-3</sup> which is very cheap and is considered a sustainable clean fuel which could substitute fossil energy sources. Therefore, its transformation to strategic compounds with high commercial values is highly desirable. However, the uncontrolled oxidation of glycerol can generate a plethora of products, as glyceric acid, glycolic acid, dihydroxyacetone, tartronic acid, glyceraldehyde, lactic acid, oxalic acid, etc.<sup>1-3</sup> Hence, selectivity towards a certain product is a key issue in this process. Nevertheless, the similarity of the reactive hydroxyl groups in the glycerol molecule is one of the difficulties encountered for the precise partial oxidation of this organic compound. The development of a novel catalyst with high conversion and high selectivity towards products with actual industrial interest<sup>2</sup> may overcome this difficulty and help to find a commercially viable application to the current excess in the production of glycerol.

Supported noble metals (Au, Pt, Pd, Rh and Ir), especially bimetallic Au-Pd and Au-Ru noble metals, have been well

investigated as catalysts for the selective oxidation of glycerol.<sup>4-17</sup> The most commonly studied supports are activated carbon and titania. Recently, bimetallic Au-Pd and Au-Ru catalysts supported on ceria-zirconia mixed oxides have also shown synergistic effect for this reaction.<sup>16, 17</sup>

Ceria and CeO<sub>2</sub>-based materials have attracted great interest both in heterogeneous catalysis<sup>18, 19</sup> and biological applications<sup>20-22</sup> due to its excellent oxygen exchange capability, related to a facile exchange between Ce<sup>3+</sup> and Ce<sup>4+</sup>. During the past 10 years, different morphologies of ceria, such as nanorods, nanocubes, nano-octahedra and nanotubes have been synthesised, being proved that they exhibit different catalytic properties compared with those of conventional ceria powders.<sup>23-25</sup> CO oxidation,<sup>26</sup> H<sub>2</sub> oxidation,<sup>27</sup> soot combustion,<sup>28, 29</sup> total oxidation of polycyclic aromatic hydrocarbons and toluene are among the reactions in which the influence of oxide morphology has been investigated.<sup>30, 31</sup> Some efforts have been made in order to study the adsorption of probe molecules, such as CO,<sup>26</sup> methanol,<sup>32</sup> CO<sub>2</sub>,<sup>33, 34</sup> pyridine,<sup>33</sup> SO<sub>2</sub> and NO<sub>x</sub><sup>34</sup> on nanoceria with different morphologies of using spectroscopic methods. On the other hand, very recently the partial catalytic oxidation of organic compounds using bare CeO<sub>2</sub> has been reported. In particular, some works dealing with selective oxidation of alcohols with only one hydroxyl functional group to their corresponding aldehydes,<sup>35-38</sup> aniline to nitrosobenzene,<sup>39</sup> (hydroxymethyl)furfuran to FDCA,<sup>40</sup> p-xylene to terephthalic acid,<sup>41, 42</sup> and styrene to styrene oxide<sup>43</sup> can be found in the literature. Until now, no selective oxidation of polyols over noble metal-free ceria nanoparticles or ceria with controlled morphologies has been studied. In this work, ceria nanocubes and ceria nanorods have been tested in the selective oxidation of glycerol and their performance has been compared with that of commercial ceria powders of both high and low surface areas.

<sup>a</sup> Departamento de Ciencia de los Materiales, Ingeniería Metalúrgica y Química Inorgánica, Facultad de Ciencias, Universidad de Cádiz, Campus Río San Pedro, Puerto Real (Cádiz), E-11510, Spain.

Email: [xiaowei.chen@uca.es](mailto:xiaowei.chen@uca.es); Tel: +34-956 012741

<sup>b</sup> Dipartimento di Chimica, Università degli Studi di Milano, Milan, I-20133, Italy

<sup>c</sup> Departamento de Física de la Materia Condensada, Facultad de Ciencias, Universidad de Cádiz, Campus Río San Pedro, Puerto Real (Cádiz), E-11510, Spain.

<sup>d</sup> Heavy Oil State Laboratory and Center for Bioengineering and Biotechnology, China University of Petroleum (East China), Qingdao, 266580, China

<sup>e</sup> † Electronic Supplementary Information (ESI) available: [details of any supplementary information available should be included here]. See DOI: 10.1039/x0xx00000x

## 2. Experimental

### 2.1. Catalysts synthesis

Two commercial ceria samples were used as references: one with a low surface area (CeO<sub>2</sub>-LS: 7 m<sup>2</sup>·g<sup>-1</sup>) from Sigma-Aldrich, and another with a high surface area (CeO<sub>2</sub>-HS: 118 m<sup>2</sup>·g<sup>-1</sup>) from Rhodia. The synthesis conditions of ceria nanocubes (CeO<sub>2</sub>-NC) have been described in our previous work.<sup>21, 22, 44, 45</sup> Part of the CeO<sub>2</sub>-NC sample was oxidized with a flow of 5%O<sub>2</sub>/He at 600 °C (CeO<sub>2</sub>-NC-O600) under the same conditions used elsewhere.<sup>44</sup> Ceria nanorods (CeO<sub>2</sub>-NR) were also synthesized using a hydrothermal method as reported by Tana et al.<sup>46</sup> For obtaining these CeO<sub>2</sub> nanorods, Ce(NO<sub>3</sub>)<sub>3</sub> (0.21 M, 100 mL) and NaOH (4 M, 125 mL) solutions, and 15 mL of MilliQ water were mixed in a Teflon-lined stainless steel autoclave of 300 mL, which was introduced in an oven. The hydrothermal reaction was carried out at 100 °C for 14 h, and the as-synthesized CeO<sub>2</sub>-NR precipitate was centrifuged, washed several times with water and once with ethanol, and dried for 16 h.

### 2.2. Characterization of the catalysts

X-ray diffraction patterns (XRD) of the samples were obtained using a D8 ADVANCE diffractometer of Bruker with Cu K $\alpha$  radiation. The angle range was from 5 to 110° and acquisition time of diagram was 1 h for each sample.

The morphology of ceria nanoparticles, and their crystalline structure were determined by High Resolution Transmission Electron Microscopy (HRTEM). The acquired HRTEM images were collected in a JEOL 2010-F microscope operating at 200 kV.

The BET specific surface areas of the samples were measured with a Micromeritics ASAP2020 via nitrogen adsorption at -196 °C. Before the analysis of nitrogen adsorption, the samples were pretreated at 150 °C for 2 h under vacuum to know the real weight of the sample.

Temperature programmed reduction (TPR) with H<sub>2</sub> and CO was performed over the ceria samples using a U-shaped quartz reactor. The samples were pretreated at 500 °C for 1 h in a flow of 5%O<sub>2</sub>/He and then cooled down to 150 °C in the same flow. Pure He was switched into the reactor and cooled down to room temperature. A flow of 5% H<sub>2</sub>/Ar or 5%CO/He with a flow rate of 60 mL·min<sup>-1</sup> was used as a reductant during H<sub>2</sub>-TPR and CO-TPR. The temperature was increased from room temperature to 950 °C with a heating rate of 10 °C·min<sup>-1</sup>. A Thermostar GSD301T1 mass spectrometer from Pfeiffer Vacuum was connected to the outlet of the reactor. The mass/charge ratios (m/z) of 18 and 44 were registered in order to monitor the formation of H<sub>2</sub>O and CO<sub>2</sub> during TPR experiments, respectively.

The X-ray Photoelectron Spectroscopy (XPS) analyses were performed with Kratos Axis Ultra DLD instrument with monochromatic Al K $\alpha$  radiation (1486.6 eV), operated with an X-ray power of 150 W. Spectra were acquired in the constant analyzer energy mode, with pass energy of 20 eV. Powder samples were pressed into pellets and stuck on a double-sided adhesive conducting tape. The samples were analysed without any pretreatment. Surface charging effects were compensated by using the Kratos coaxial neutralization system. Binding energy scale was calibrated with respect to the C 1s signal at 284.8 eV. Spectra

interpretation and decomposition was performed on CasaXPS software (version 2.3.19rev1.1m, 2017 Casa Software Ltd.).

Raman spectra of the ceria samples were measured using a confocal dispersive Raman spectrometer (Jasco, model NRS-7200) in backscattering configuration. A 532 nm Nd-YAG laser operating at 5.6 mW power was used as excitation source. The laser beam was focused on the samples by a 100X microscope objective, with spot size of about 1  $\mu$ m diameter.

### 2.3. Catalytic tests of glycerol oxidation

Catalytic reactions of glycerol oxidation were carried out in a 30 mL glass reactor equipped with a thermostat and an electronically controlled magnetic stirrer connected to a 5000 mL reservoir charged with oxygen (3 atm.).

Glycerol 0.3 M, and the catalyst (glycerol/catalyst = 5/1 (wt/wt)) were mixed in distilled water (total volume is 10 mL) and 4 equivalent of NaOH. The reactor was pressurized at 3 atm of oxygen and set to 50 °C. Once the temperature was reached, the monitoring of the reaction started. The reaction was initiated by stirring.

Samples were removed periodically and analyzed by high-performance liquid chromatography (HPLC) using a column (Alltech OA-10308, 300 mm, 7.8 mm) with UV and refractive index (RI) detection to analyze the mixture of the samples. Aqueous H<sub>3</sub>PO<sub>4</sub> solution (0.1 wt%) was used as the eluent. Products were identified by comparison with the original samples. Hydrogen peroxide produced after reaction was quantified by permanganate titration. A sample (5 mL) of the filtered reacting solution (after 30 minutes of reaction) was titrated with a 0.01 N KMnO<sub>4</sub>. The detection limit of H<sub>2</sub>O<sub>2</sub> was 0.01 mM.

Recycling tests were carried out under the same experimental conditions. The catalyst was recycled in the subsequent run after filtration without any further treatment. The recovery of the catalyst was always more than 95%.

## 3. Results and Discussion

Figure 1 displays the XRD diagrams of all ceria samples, which present a fluorite-like, face-centered cubic structure (Fm-3m) characteristic of ceria in all cases. The X-ray diffraction peaks of CeO<sub>2</sub>-NR are much wider than those of the rest of ceria samples. This result suggests that the crystallite size of CeO<sub>2</sub>-NR is the smallest among all samples.

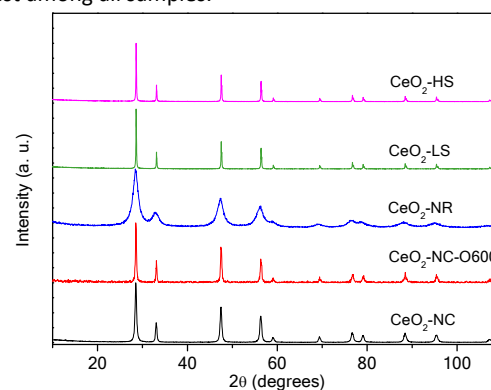
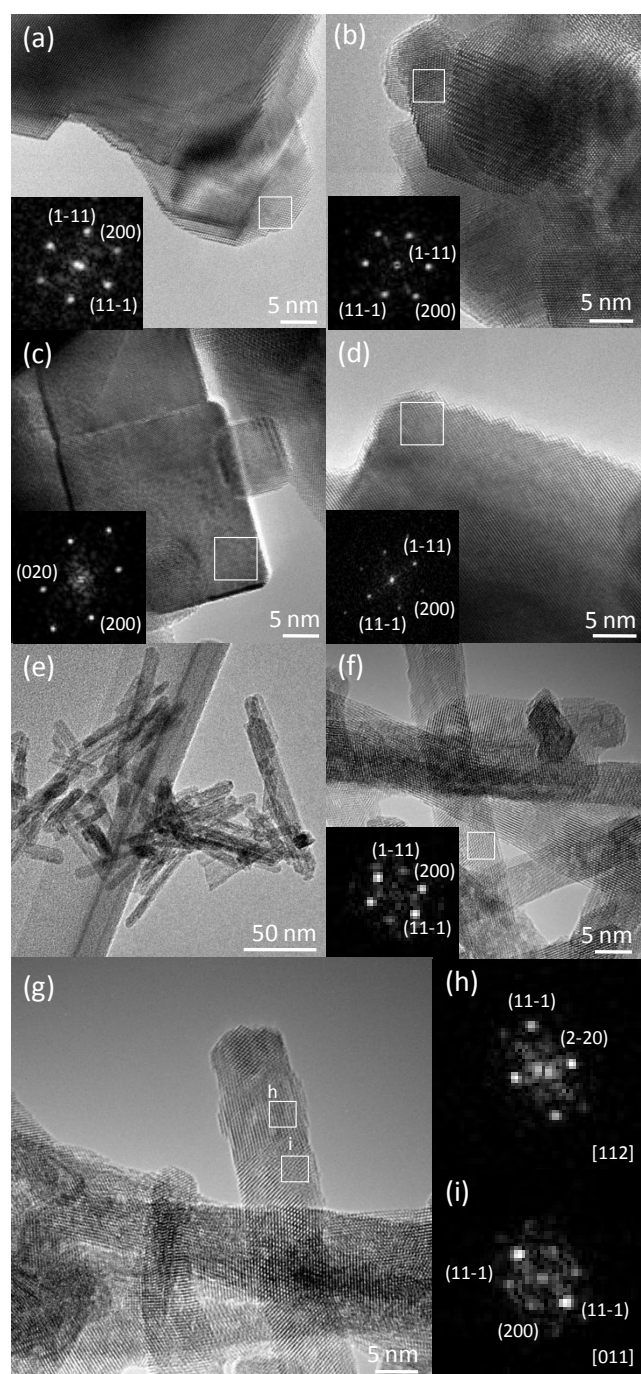


Figure 1 Normalized XRD patterns of all the ceria samples.



**Figure 2** TEM images of (a) CeO<sub>2</sub>-LS, (b) CeO<sub>2</sub>-HS, (c) CeO<sub>2</sub>-NC, (d) CeO<sub>2</sub>-NC-O600, and (e) - (i) CeO<sub>2</sub>-NR.

Figures 2a and 2b show representative TEM images of the CeO<sub>2</sub>-LS and CeO<sub>2</sub>-HS samples, indicating that they are constituted by irregularly shaped crystallites bounded by a variety of planes of different crystallography, including {100} and {111}, among many others. Figure 2c clearly illustrates the cubic shape of CeO<sub>2</sub>-NC nanocrystals, which are mainly enclosed by {100} surfaces. The edge lengths of CeO<sub>2</sub>-NC crystallites fall in the 5-50 nm range. Likewise, it leads to the transformation of {110} facets into a system of {111} tiny facets, which will be referred to nanofacets in the following text. The growth of these nanofacets imprints a zigzagged aspect to the crystallite surface when observed in projection, (Figure 2d), as

previously reported.<sup>44</sup> Importantly, the BET specific surface area of CeO<sub>2</sub>-NC decreases from 38 to 18 m<sup>2</sup>·g<sup>-1</sup> after oxidation at 600 °C.

After careful measurements, the percentage of surface corresponding to each type of facet in both CeO<sub>2</sub>-NC and CeO<sub>2</sub>-NC-O600 samples was estimated.<sup>44</sup> The dominant {100} facet decreases from 84% to 75% after oxidation, while {110} facets increase from 16 to 24%. Concerning {111} facets, they originally are only located at the corners of the nanocubes in CeO<sub>2</sub>-NC, where they represent a negligible fraction of the surface, but their contribution increases up to 1% in CeO<sub>2</sub>-NC-O600. Additionally, the majority of {110} facets on the edges of nanocubes were converted into zig-zag shaped {111} nanofacets during the oxidation treatment. Hence, this increases the total contribution of {111} and {110} facets on the surface of the CeO<sub>2</sub>-NC-O600 sample to nearly 25%. As shown in Figures 2e - 2g, the diameters of CeO<sub>2</sub>-NR are below 10 nm. The BET specific surface area of this sample is 140 m<sup>2</sup>·g<sup>-1</sup>, which is slightly higher than that of the commercial CeO<sub>2</sub>-HS with high surface area. As it can be appreciated in the HREM image of Figure 2f, the surface of these NRs is rather rough and defective, depicting a large density of surface steps and nanopores. For example, in Figure 2g a nanorod with two adjacent crystallographic domains which present different exposed surfaces and even grew along different axes, can be observed. Therefore, the surface of these nanorods cannot be naively assigned to the expected mixture of {110} and {100} planes, as previously reported.<sup>46-48</sup> The surface crystallography of this sample is much more complex, and the presence of these defects can significantly modify its redox and catalytic behaviour.<sup>26</sup>

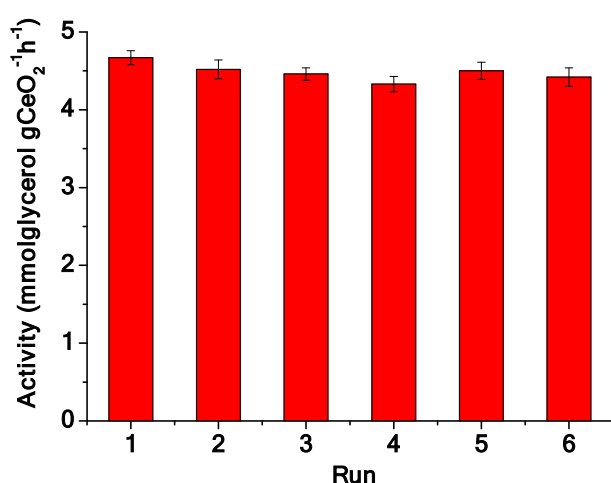
Table 1 lists the activity and selectivity values for glycerol oxidation over all the investigated ceria catalysts. Activities are expressed as an average value, i.e. as converted mmol glycerol per gram of ceria per hour (mmol<sub>glycerol</sub>·g<sup>-1</sup>·h<sup>-1</sup>) and converted mmol glycerol per square meter of ceria per hour (mmol<sub>glycerol</sub>·m<sup>-2</sup>·h<sup>-1</sup>). The blank experiment indicates that there is no glycerol conversion without any catalyst in the autoclave after 6 h of reaction time.

In terms of mmol<sub>glycerol</sub>·g<sup>-1</sup>·h<sup>-1</sup>, the highest activity of glycerol oxidation among all the studied ceria samples was found over CeO<sub>2</sub>-NR catalyst (4.67 mmol<sub>glycerol</sub>·g<sup>-1</sup>·h<sup>-1</sup>), probably because it presents the highest surface area (140 m<sup>2</sup>·g<sup>-1</sup>). However, CeO<sub>2</sub>-HS (0.72 mmol<sub>glycerol</sub>·g<sup>-1</sup>·h<sup>-1</sup>), which has a similar surface area (118 m<sup>2</sup>·g<sup>-1</sup>), is much less active than CeO<sub>2</sub>-NR. Furthermore, CeO<sub>2</sub>-HS even presents only half of the catalytic activity of CeO<sub>2</sub>-NC (1.57 mmol<sub>glycerol</sub>·g<sup>-1</sup>·h<sup>-1</sup>), which has a much lower surface area (38 m<sup>2</sup>·g<sup>-1</sup>). These results suggest that surface crystallography should play a more important role in the catalytic activity of ceria for the partial oxidation of glycerol than exposed surface area. This is further confirmed by the results obtained using the two nanocube samples: CeO<sub>2</sub>-NC-O600 sample duplicates the activity (3.04 mmol<sub>glycerol</sub>·g<sup>-1</sup>·h<sup>-1</sup>) of CeO<sub>2</sub>-NC in spite that the surface area of the former is lower (18 m<sup>2</sup>·g<sup>-1</sup>).

To evaluate the contribution of the total exposed surface area in the catalytic activities, and to unveil the effects of the crystallographic nature of the surface in the partial oxidation of glycerol, the activity values were normalized to exposed m<sup>2</sup> of ceria (Table 1). Note that on this basis the most active catalyst is CeO<sub>2</sub>-NC-O600 (0.169 mmol<sub>glycerol</sub>·m<sup>-2</sup>·h<sup>-1</sup>) followed by CeO<sub>2</sub>-NC (0.041 mmol<sub>glycerol</sub>·m<sup>-2</sup>·h<sup>-1</sup>) and CeO<sub>2</sub>-NR (0.033 mmol<sub>glycerol</sub>·m<sup>-2</sup>·h<sup>-1</sup>). The commercial ceria nanoparticles show significantly lower activities per surface unit than ceria nanocubes and nanorods, 0.014 and 0.006 mmol<sub>glycerol</sub>·m<sup>-2</sup>·h<sup>-1</sup>, for CeO<sub>2</sub>-LS and CeO<sub>2</sub>-HS, respectively.

Table 1 Glycerol oxidation over ceria nanocubes and nanorods catalysts<sup>a</sup>View Article Online  
DOI: 10.1039/C9CY00273A

Catalyst	S <sub>BET</sub> (m <sup>2</sup> ·g <sup>-1</sup> )	Ce <sup>3+</sup> (mol%) <sup>b</sup>	Activity (mmol <sub>glycerol</sub> ·g <sup>-1</sup> ·h <sup>-1</sup> )	Activity (mmol <sub>glycerol</sub> ·m <sup>-2</sup> ·h <sup>-1</sup> )	Selectivity (%)			
					Glyceric acid	Glycolic acid	Formate	Tartronic acid
No-catalyst			-		-	-	-	
CeO <sub>2</sub> -LS	7	7	0.10	0.014	78	10	6	-
CeO <sub>2</sub> -HS	118	7	0.72	0.006	70	15	12	2
CeO <sub>2</sub> -NC	38	9	1.57	0.041	35	42	23	-
CeO <sub>2</sub> -NC-O600	18	7	3.04	0.169	30	42	27	-
CeO <sub>2</sub> -NR	140	13	4.67	0.033	66	22	6	5

<sup>a</sup> Reaction conditions: Glycerol 0.3 M, glycerol/catalyst=5/1 (wt/wt), 50 °C, 1250 rpm, 3 bar O<sub>2</sub>, 4 eq NaOH.<sup>b</sup> Ce<sup>3+</sup> percentages in total amount of Ce were calculated by XPS data.**Figure 3** Stability in the selective oxidation of glycerol over CeO<sub>2</sub>-NR.

A higher activity of ceria crystallites with {100}/{110} dominating planes, like nanocubes, has been also observed for other reactions like CO oxidation,<sup>47</sup> toluene oxidation<sup>36</sup> or benzyl alcohol oxidation.<sup>37</sup> This has been attributed to the high surface energy of {100} facets and to the presence of a high concentration of oxygen vacancies on the surface of the nanocubes. A dramatic effect of the surface reconstruction onto the activity of the nanocubes for the selective oxidation of glycerol can be also observed in the Table 1. Thus, although oxidation at 600 °C leads to a significant reduction of the total available surface, activity per gram of ceria increases to double amount, while intrinsic activity per m<sup>2</sup> is nearly four times higher than the untreated ceria nanocube sample. Therefore, our results emphasize that the formation of {111} nanofacets on the CeO<sub>2</sub>-NC-O600 sample seems crucial for the observed drastic increase in catalytic activity with respect to the CeO<sub>2</sub>-NC sample.

In terms of selectivity, we observed that CeO<sub>2</sub> nanoparticles (CeO<sub>2</sub>-LS and CeO<sub>2</sub>-HS) and ceria nanorods (CeO<sub>2</sub>-NR), which do not depict preferential exposed planes, show glyceric acid as the major product (66-78%). Hence, these samples allow a deeper oxidation to C3 tartronic acid (Table 1) without C-C cleavage. In

contrast, ceria nanocubes promoted C-C bond cleavage, with formation of C2 (glycolic acid 42%) and C1 (formate 23-27%) as the main products. Literature has shown that, for Au catalysts, C-C cleavage can be correlated with the amount of native H<sub>2</sub>O<sub>2</sub> produced during the reaction, that is, higher selectivity towards glycolic and formic acid when a higher amount of H<sub>2</sub>O<sub>2</sub> was formed.<sup>49, 50</sup> Therefore, we determined the amount of H<sub>2</sub>O<sub>2</sub> present during the reaction by titration with KMnO<sub>4</sub>, using CeO<sub>2</sub>-NR and CeO<sub>2</sub>-NC as representative catalysts. When the CeO<sub>2</sub>-NR was employed as a catalyst, very little amount of H<sub>2</sub>O<sub>2</sub> was detected (0.012 mmol·L<sup>-1</sup>). On the contrary, much higher amount of H<sub>2</sub>O<sub>2</sub> was detected (0.26 mmol·L<sup>-1</sup>) in the case of CeO<sub>2</sub>-NC. And thus, the different selectivity observed using different CeO<sub>2</sub> catalysts can be attributed to the presence of a different amount of native H<sub>2</sub>O<sub>2</sub>. CeO<sub>2</sub>-NC, which shows a high selectivity towards C2+C1 products (42% and 23% for glycolic and formic acid, respectively), produces 20 times more H<sub>2</sub>O<sub>2</sub> than CeO<sub>2</sub>-NR (22% and 6% for glycolic and formic acid, respectively) (Table 1).

The stability in the selective oxidation of glycerol over CeO<sub>2</sub>-NR, which is the most active catalyst for this reaction, has been evaluated. As shown in Figure 3, no deactivation was observed even after 6 consecutive reaction cycles, which is a very promising result.

Figure 4 demonstrates the temperature programmed reduction with H<sub>2</sub> (H<sub>2</sub>-TPR) profiles of all the ceria samples. For the CeO<sub>2</sub>-LS sample, there is only one reduction peak at 834 °C. Two reduction peaks appear at 525 and 834 °C for the CeO<sub>2</sub>-HS, CeO<sub>2</sub>-NC, and CeO<sub>2</sub>-NR samples. However, the two reduction temperatures of CeO<sub>2</sub>-NC-O600 are 550 and 869 °C, slightly at higher temperatures than those of the other samples.

Temperature programmed reduction with CO has been also performed over the different ceria samples, Figure S1. Compared to H<sub>2</sub>-TPR results, the CO<sub>2</sub> desorption peaks appear at lower temperatures. The first CO<sub>2</sub> formation peak in all the ceria samples falls in the 300 to 430 °C range, starting at 150 °C. The low release temperature of CO<sub>2</sub> during CO-TPR can be attributed to the reaction CO with active lattice oxygen on the surface of ceria.<sup>26</sup> The second CO<sub>2</sub> evolution peak is located from 780 to 870 °C, which can be assigned to CO reaction with both surface hydroxyl groups and lattice oxygen.<sup>26</sup> Therefore, there is no clear, direct, connection between the redox properties of these

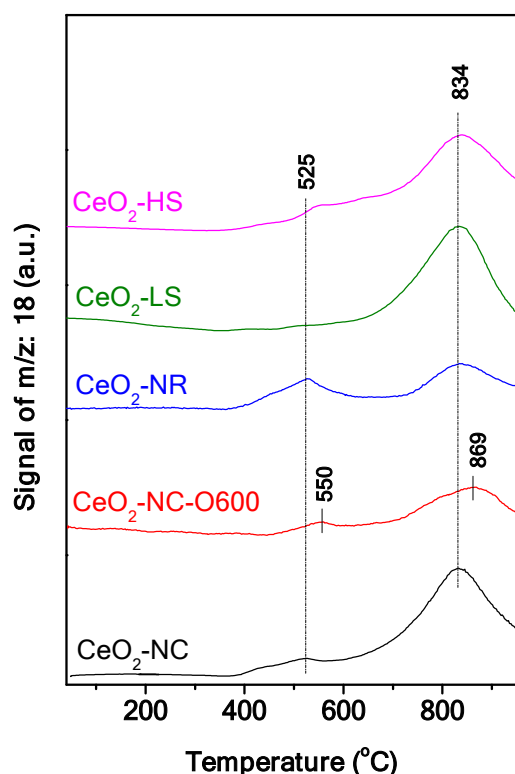


**Figure 4** H<sub>2</sub>O formation during H<sub>2</sub>-Temperature Programmed Reduction experiments of all the ceria samples.

ceria samples using both H<sub>2</sub> and CO as reductants and their catalytic activity or selectivity for selective oxidation of glycerol.

Figure S2 shows XPS spectra of Ce3d core level of all the ceria samples. The percentages of Ce<sup>3+</sup> at the surface layers of these catalysts are listed in Table 1. The value observed for CeO<sub>2</sub>-HS and CeO<sub>2</sub>-LS amounts to 7%, which is quite close to that in the CeO<sub>2</sub>-NC catalyst, 9%. When the CeO<sub>2</sub>-NC catalyst is oxidized at 600 °C, the Ce<sup>3+</sup> percentage decreases slightly to 7%. However, Ce<sup>3+</sup> percentage in CeO<sub>2</sub>-NR increases up to 13%, which is almost double the amount observed in both the commercial CeO<sub>2</sub> and ceria nanocube samples. The comparison of the CeO<sub>2</sub>-HS and CeO<sub>2</sub>-NR samples, which show quite close surface areas, indicates that the oxidation state of the surface may be one of the factors influencing catalytic activity in this reaction on pure ceria.

To get further structural information, Raman spectra of all the ceria samples were also recorded, Figure 5. Similar to XPS results, no significant difference between commercial CeO<sub>2</sub> and CeO<sub>2</sub> nanocube samples was observed. The F<sub>2g</sub> symmetrical stretching vibration mode of CeO<sub>2</sub> invariably appears around 466 cm<sup>-1</sup> for these samples, with high intensity and low value for FWHM, as previously reported in the literature.<sup>26, 51, 52</sup> However, CeO<sub>2</sub>-NR catalyst shows a notable shift of the F<sub>2g</sub> band towards lower frequencies (461 cm<sup>-1</sup>), larger values of FWHM, and a strong catalyst shows a notable shift of the F<sub>2g</sub> band towards lower reduction of the intensity for the same collection times, in comparison with the other ceria samples.

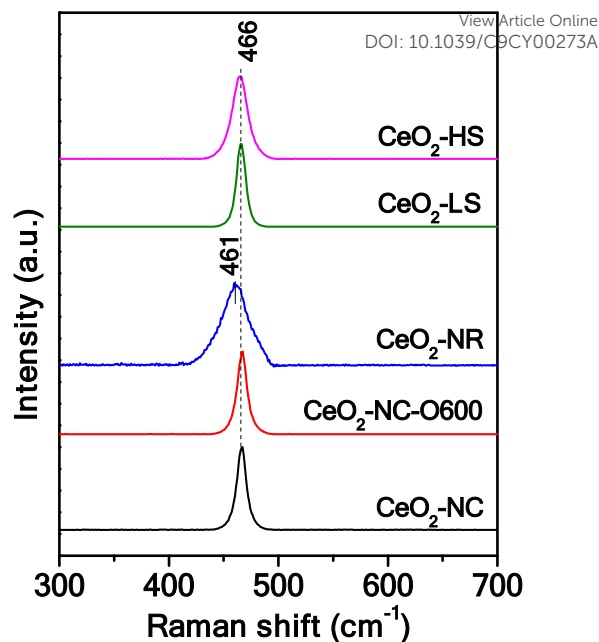


**Figure 5** Normalized Raman spectra of all the ceria samples.

Such differences in the F<sub>2g</sub> Raman band are presumably a size-dependent phenomenon of the ceria particles and a contribution of inhomogeneous strain, which result in broadening associated with dispersion in particle size and phonon confinement.<sup>52</sup> No indications of the Raman band at 592 cm<sup>-1</sup>, which has been assigned to oxygen vacancy of CeO<sub>2</sub>, was observed in none of the ceria samples studied in this work. Therefore, apart from differences in crystal size, no evidence of a much larger defect content between the different samples was evident.

#### 4. Conclusions

The successful usage of different ceria nanocatalysts for glycerol oxidation reaction has been presented here. Among all the investigated samples, CeO<sub>2</sub> nanorods stand as the most active on a per gram of ceria basis, simply due to its higher surface area. On the other hand, selectivity towards different products significantly changes between samples. The whole set of characterization data indicate that, although the presence of reduced Ce<sup>3+</sup> species contributes to the activity in this reaction, the peculiarities of the interactions of the reactants with surfaces of differing crystallographic nature is the major influencing factor in the catalytic activity of these materials.

In particular, our results confirm that {100} surfaces feature a higher intrinsic activity than conventional, extended, {111} planes. However, the development of a system of {111} nanofacets seems to be at the roots of the highest intrinsic, per unit-surface, activity value observed among the whole set of oxide morphologies for the partial oxidation of glycerol.

#### Conflicts of interest

There are no conflicts to declare.

## Acknowledgements

This work has been supported by the Ministry of Science, Innovation and Universities of Spain with reference numbers of ENE2017-82451-C3-2-R, MAT2016-81118-P and MAT2017-87579-R. X. Chen thanks the "Ramón y Cajal" Program from MINECO/FEDER of Spain. M. Tinoco acknowledges FPU Grants Program from the Spanish Ministry of Science, Innovation and Universities.

## Notes and references

- 1 B. Katryniok, H. Kimura, E. Skrzyńska, J.S. Girardon, P. Fongarland, M. Capron, R. Ducoulombier, N. Mimura, S. Paul and F. Dumeignil, *Green Chem.*, 2011, **13**, 1960-1979
- 2 M. Pagliaro, R. Ciriminna, H. Kimura, M. Rossi and C. Della Pina, *Angew. Chem. Int. Ed.*, 2007, **46**, 4434-4440
- 3 M. Besson and P. Gallezot, *Catal. Today*, 2000, **57**, 127-141
- 4 R. Garcia, M. Besson and P. Gallezot, *Appl. Catal., A.*, 1995, **127**, 165-176
- 5 S. Carrettin, P. McMorn, P. Johnston, K. Griffin and G.J. Hutchings, *Chem. Commun.*, 2002, **7**, 696-697
- 6 S. Carrettin, P. McMorn, P. Johnston, K. Griffin, C.J. Kiely and G.J. Hutchings, *Phys. Chem. Chem. Phys.*, 2003, **5**, 1329-1336
- 7 E.G. Rodrigues, M.F.R. Pereira, X. Chen, J.J. Delgado and J.J.M. Órfão, *J. Catal.*, 2011, **281**, 119-127
- 8 E.G. Rodrigues, M.F.R. Pereira, J.J. Delgado, X. Chen and J.J.M. Órfão, *Catal. Commun.*, 2011, **16**, 64-69
- 9 E.G. Rodrigues, S.A.C. Carabineiro, J.J. Delgado, X. Chen, M.F.R. Pereira and J.J.M. Órfão, *J. Catal.*, 2012, **285**, 83-91
- 10 E.G. Rodrigues, J.J. Delgado, X. Chen, M.F.R. Pereira and J.J.M. Órfão, *Ind. Eng. Chem. Res.*, 2012, **51**, 15884-15894
- 11 E.G. Rodrigues, S.A.C. Carabineiro, X. Chen, J.J. Delgado, J.L. Figueiredo, M.F.R. Pereira and J.J.M. Órfão, *Catal. Lett.*, 2011, **141**, 420-431
- 12 A. Villa, C. Campione and L. Prati, *Catal. Lett.*, 2007, **115**, 133-136
- 13 D. Wang, A. Villa, F. Porta, D. Su and L. Prati, *Chem. Commun.*, 2006, 1956-1958
- 14 D. Wang, A. Villa, F. Porta, L. Prati and D. Su, *J. Phys. Chem. C*, 2008, **112**, 8617-8622
- 15 L. Prati, A. Villa, F. Porta, D. Wang and D. Su, *Catal. Today*, 2007, **122**, 386-390
- 16 C.M. Olmos, L.E. Chinchilla, E.G. Rodrigues, J.J. Delgado, A.B. Hungria, G. Blanco, M.F.R. Pereira, J.J.M. Órfão, J.J. Calvino and X. Chen, *Appl. Catal., B.*, 2016, **197**, 222-235
- 17 L.E. Chinchilla, C.M. Olmos, A. Villa, A. Carlsson, L. Prati, X. Chen, G. Blanco, J.J. Calvino and A.B. Hungria, *Catal. Today*, 2015, **253**, 178-189
- 18 A. Trovarelli, *Cat. Rev. - Sci. Eng.*, 1996, **38**, 439-520
- 19 C. Sun, H. Li and L. Chen, *Energy Environ. Sci.*, 2012, **5**, 8475-8505
- 20 F. Pagliari, C. Mandoli, G. Forte, E. Magnani, S. Pagliari, G. Nardone, S. Licocchia, M. Minieri, P. Di Nardo and E. Fraversari, *ACS Nano*, 2012, **6**, 3767-3775
- 21 S. Fernandez-Garcia, L. Jiang, M. Tinoco, A.B. Hungria, J. Han, G. Blanco, J.J. Calvino and X. Chen, *J. Phys. Chem. C*, 2016, **120**, 1891-1901
- 22 L. Jiang, S. Fernandez-Garcia, M. Tinoco, Z. Yan, Q. Xue, G. Blanco, J.J. Calvino, A.B. Hungria and X. Chen, *ACS Appl. Mater. Interfaces*, 2017, **9**, 18595-18608
- 23 K. Zhou and Y. Li, *Angew. Chem. Int. Ed.*, 2012, **51**, 602-613
- 24 C. Sun, H. Li, H. Zhang, Z. Wang and L. Chen, *Nanotechnology*, 2005, **16**, 1454-1463
- 25 S. C. Sun, H. Li, Z. Zhang, L. Chen and X. Huang, *Chem. Letters*, 2004, **33**, 662-663
- 26 Z. Wu, M. Li and S.H. Overbury, *J. Catal.*, 2012, **285**, 61-73
- 27 T. Désaunay, G. Bonura, V. Chiodo, S. Freni, J.P. Couzinié, J. Bourgon, A. Ringuedé, F. Labat, C. Adamo and M. Cassir, *J. Catal.*, 2013, **297**, 193-201
- 28 E. Aneggi, D. Wiaterski, C. De Leitenburg, J. Llorca and A. Trovarelli, *ACS Catal.*, 2014, **4**, 172-181
- 29 T. Andana, M. Piumetti, S. Bensaid, N. Russo, D. Fino and R. Pirone, *Appl. Catal., B.*, 2016, **197**, 125-137
- 30 L. Torrente-Murciano, A. Gilbank, B. Puertolas, T. Garcia, B. Solsona and D. Chadwick, *Appl. Catal., B.*, 2013, **132-133**, 116-122
- 31 J.M. López, A.L. Gilbank, T. García, B. Solsona, S. Agouram and L. Torrente-Murciano, *Appl. Catal., B.*, 2015, **174-175**, 403-412
- 32 Z. Wu, M. Li, D.R. Mullins and S.H. Overbury, *ACS Catal.*, 2012, **2**, 2224-2234
- 33 Z. Wu, A.K.P. Mann, M. Li and S.H. Overbury, *J. Phys. Chem. C*, 2015, **119**, 7340-7350
- 34 U. Tumuluri, G. Rother and Z. Wu, *Ind. Eng. Chem. Res.*, 2016, **55**, 3909-3919
- 35 M. Li, Z. Wu and S.H. Overbury, *J. Catal.*, 2013, **306**, 164-176
- 36 J. Lv, Y. Shen, L. Peng, X. Guo and W. Ding, *Chem. Commun.*, 2010, **46**, 5909-5911
- 37 K. Deori, C. Kalita and S. Deka, *J. Mater. Chem. A*, 2015, **3**, 6909-6920
- 38 J. E. Sutton, T. Danielson, A. Beste and A. Savara, *J. Phys Chem Lett.*, 2017, **8**, 5810-5814
- 39 A.G.M. da Silva, D.C. Batalha, T.S. Rodrigues, E.G. Candido, S.C. Luz, I.C. de Freitas, F.C. Fonseca, D.C. de Oliveira, J.C. Taylor, S.I. Córdoba de Torresi, P.H.C. Camargo and H.V. Fajardo, *Catal. Sci. Technol.*, 2018, **8**, 1828-1839
- 40 M. Ventura, F. Nocito, E. de Gliglio, S. Cometa, A. Altomare and A. Dibenedetto, *Green Chem.*, 2018, **20**, 3921-3926
- 41 K. Deori, D. Gupta, B. Saha and S. Deka, *ACS Catal.*, 2014, **4**, 3169-3179
- 42 K. Deori, D. Gupta, B. Saha, S.K. Awasthi and S. Deka, *J. Mater. Chem.*, 2013, **1**, 7091-7099
- 43 P. Pal, S.K. Pahari, A. Sinhamahapatra, M. Jayachandran, G.V.M. Kiruthika, H.C. Bajaj and A.B. Panda, *RSC Adv.*, 2013, **3**, 10837-10847
- 44 M. Tinoco, S. Fernandez-Garcia, M. Lopez-Haro, A.B. Hungria, X. Chen, G. Blanco, J.A. Perez-Omil, S.E. Collins, H. Okuno and J.J. Calvino, *ACS Catal.*, 2015, **5**, 3504-3513

## Journal Name

## COMMUNICATION

- 45 S. Fernandez-Garcia, S.E. Collins, M. Tinoco, A.B. Hungría, J.J. Calvino M.A. Cauqui and X. Chen, *Catal. Today*, 2019, DOI: <https://doi.org/10.1016/j.cattod.2019.01.078>
- 46 Tana, M. Zhang, J. Li, H. Li, Y. Li and W. Shen, *Catal. Today*, 2009, **148**, 179-183
- 47 H. Mai, L. Sun, Y. Zhang, R. Si, W. Feng, H. Zhang, H. Liu and C. Yan, *J. Phys. Chem. B*, 2005, **109**, 24380-24385
- 48 N. Du, H. Zhang, B. Chen, X. Ma and D. Yang, *J. Phys. Chem. C*, 2007, **111**, 12677-12680
- 49 W. C. Ketchie, Y. L. Fang, M. S. Wong, M. Murayama and R. J. Davis, *J Catal*, 2007, **250**, 94-101
- 50 D. Wang, A. Villa, D. Su, L. Prati and R. Schlögl, *ChemCatChem* 2013, **5**, 2717-2723
- 51 Z. Wu, M. Li, J. Howe, H.M. Meyer and S.H. Overbury, *Langmuir*, 2010, **26**, 16595-16606
- 52 L. Li, G. Hu, J. Lu and M. Luo, *Acta Phys. -Chim. Sin.*, 2012, **28**, 1012-1020

View Article Online  
DOI: 10.1039/C9CY00273A

## Table of Contents

View Article Online  
DOI: 10.1039/C9CY00273A

It is reported, for the first time, that morphology controlled ceria without any addition of other metal exhibits catalytic activity for selective oxidation of glycerol. Moreover, development of {111} nanofacets plays an important role in both activity and selectivity.

